Retroemission by a glass bead monolayer for high-sensitivity, long-range imaging of upconverting phosphors

Bjørnar Sandnes,[1,2] Tim A. Kelf,[1] Hua Liu,[1] and Andrei V. Zvyagin[1,*]

[1]*MQ Biofocus Research Centre, Macquarie University, NSW 2109, Australia*

[2]*Department of Physics, University of Oslo, P.O. Box 1048 Blindern, 0316 Oslo, Norway*

**Corresponding author: andrei.zvyagin@mq.edu.au*

Received May 25, 2011; accepted June 29, 2011;
posted July 11, 2011 (Doc. ID 148186); published August 1, 2011

We introduce a retroemitter (REM) device comprising a planar glass bead set placed on a luminescent material substrate, which converges an excitation beam into a set of foci (voxels). The in-voxel emission is collimated by the beads, and propagates upstream over the long range, unlike the out-of-voxel emission spreading in all angles. The REM signal contrast is characterized as a function of incidence and observation angles and propagation distance. REM signal contrasts of approximately 20 and 1600 were found for the organic fluorescent dye and upconverting phosphor substrates, respectively. In the latter case, nonlinear optical signal enhancement plays a role in addition to the retroemission effect. This allows centimeter-scale REM patterns to be read out at the meter-scale distance using eye-safe sub-mW/cm^2 excitation intensities.

OCIS codes: 280.1415, 180.1790, 160.2540, 160.4330.

Three main modalities of the optical scanning microscopies, the reflection scanning confocal microscopy [1], (epi)fluorescence scanning confocal microscopy [2], and nonlinear optical microscopy [3], have a common property of sampling focal volume (voxel) content by means of spatial frequency filtering. Elastic or inelastic scattering/emission in the voxel is usually refocused at a pinhole, which preferentially selects the signal spatial frequencies. Transformation of the in-voxel emission into a low-convergence quasi-plane wave, referred to as autocollimation, is a prerequisite for realization of this pinhole filtering. Hence, the optical scanning microscopy can be viewed as a retroreflector, or, more generally, a retroemitter (REM) system, where the optical energy conversion (via elastic scattering, fluorescence, nonlinear processes) occurs at the voxel. The optical sectioning property of the optical scanning microscopy corresponds to the autocollimation property of the REM system.

The retroemission aspect of optical scanning microscopy becomes more apparent in the case where the role of the focusing element is delegated to a set of miniature lenses or beads [4]. This REM system possesses several interesting and useful properties [5]. First, since the retroemitted beam returns along the incoming excitation path, it is, in the first approximation, independent of the angular tilt of the REM planar device. Second, due to the collimation of the retroemitted beam, it gains the ability to propagate over large distances, unlike the out-of-voxel emission that attenuates according to the inverse square law, i.e., $\sim d^{-2}$, where d is the distance between the REM and imaging devices. Hence, the REM signal contrast is increased versus d. Arranging miniature beads in a monolayer pattern on a luminescence substrate allows encoding information that can be read out at the meter-scale distance. In the case of nonlinear optical materials, in addition to the REM signal contrast enhancement due to the autocollimation, a contribution from the signal dependence on I^p, where I is the optical intensity and p is the nonlinear effect order, plays a considerable role, in analogy with nonlinear optical microscopy. Upconverting phosphors (UCPs) are of a particular note due to their high nonlinear conversion efficiency; for example, a few luminescent photons in the visible spectral range are generated per 50 pairs of the absorbed IR photons [6]. A recent breakthrough in the synthesis of nanometer-size UCP nanoparticles brought these materials to the research frontier [7], especially in the biomedical area [8]. Despite their outstanding luminescence properties, which afford almost complete suppression of the biological tissue autofluorescence, high-sensitivity readout of UCP-based molecular reporters remains a bottleneck problem [9]. The proposed REM technology has potential to counter this problem. Modeling and experimental demonstration of such an optical device are addressed in this Letter.

Initially, we consider optical characteristics of a planar REM device on a linear (in a sense of $p = 1$) fluorescent substrate. The excitation was provided by an expanded 532 nm laser beam positioned 2 m from the sample [Fig. 1(a)]. A CCD camera with a variable focal length lens (7–70 mm) was positioned at an observation angle θ with respect to the excitation. The REM signal was also investigated versus the sample tilt angle, ϕ, defined as the angle between the excitation beam axis and a normal to the sample plane.

The REM device consisted of a fluorescent sheet (orange fluoroboard, Quill) covered by a monolayer of barium titanate glass spheres (Flex-O-Lite, Potters Ind.) [Fig. 1(b)], with a refractive index of 1.90–1.92, and a sphere diameter range of 0.6–0.85 mm. The glass spheres were bonded to the substrate with a thin ($>50\,\mu$m) adhesive layer, and pressed into the (wet) adhesive to come in close contact with the substrate. Figure 1(c) illustrates the contrast between a region covered with spheres (REM) and the adjacent plain fluorescent substrate (ref), with a section of the nonfluorescent background (bg) shown in the top tile. Note that the REM region is

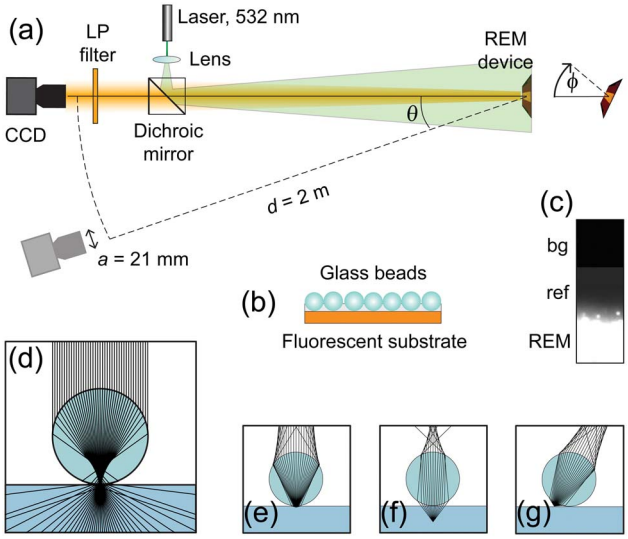

Fig. 1. (Color online) (a) Experimental setup. A diverging laser beam reflects off the dichroic mirror, and illuminates the REM device. The retroemission beam propagates upstream (leftward), through the dichroic and a long pass filter (blocking the reflected laser light), and is detected by the CCD camera. Observation, θ, and incidence angles, ϕ, are shown. (b) REM device: high-refractive-index glass spheres bonded to a fluorescent substrate. (c) CCD image illustrating signal levels from background (bg), plain fluorescent substrate (ref), and REM. Individual beads can be seen at the interface. (d) Simulation showing the focusing of parallel excitation rays by the sphere. (e) Autocollimated rays emitted at the focal point. (f) Emission outside the focal point results in noncollimated rays. (g) Autocollimated REM beam at nonzero incidence angle.

overexposed in this CCD image; quantification of signal ratios required separate exposures with exposure times generally 10–20 times shorter for the REM device compared to the fluorescent reference.

Using ray tracing simulation software developed in house, we modeled an individual sphere focusing a collimated excitation beam into micrometer-scale voxels [Fig. 1(d)]. Excited fluorescence was assumed isotropic and proportional to I. The emitted fluorescence from each voxel was subsequently mapped back through the sphere to observe the resultant far-field intensity profile. Figure 1(e) illustrates the recollimation of the emitted light from the focal point of the sphere (refractive index 1.9), where, for visual clarity, only rays intersecting the sphere are shown. Figures 1(f) and 1(g) show rays resulting from emission outside of the focal region, and REM autocollimation for tilted substrates, respectively.

Figure 2(a) shows simulation results for the REM intensity as a function of the sphere refractive index, n. $n \sim 1.9$ is optimal (for an air/glass frontal sphere interface), since the focal point is well defined and located only $\sim 15\,\mu$m behind the $600\,\mu$m sphere back surface (approaching Maxwell's cat's eye device), thereby maximizing the collection angle. The simulation showed that the refractive index of the adhesive layer had a negligible effect on the results for high-index beads.

The REM device autocollimates the emitted fluorescence into a narrow cone of light propagating upstream along the excitation path. Figure 2(b) shows the cross section of the retroemitted light, measured by varying

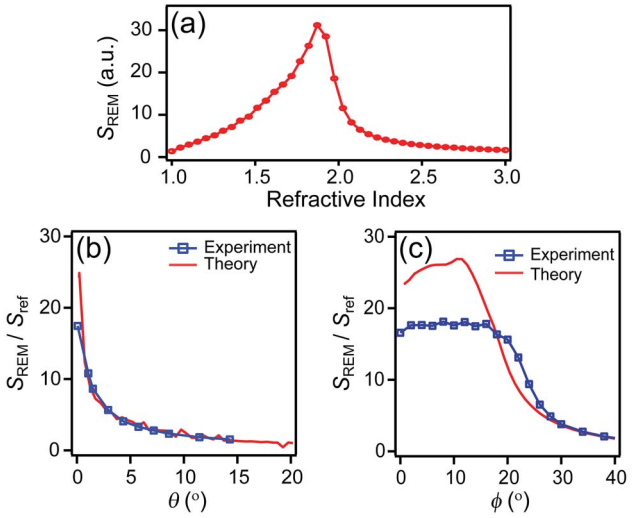

Fig. 2. (Color online) (a) Simulated REM signal as a function of bead refractive index. (b) Ratio between REM and reference signals as a function of observation angle θ. (c) Ratio between REM and reference signals as a function of angle of incidence ϕ.

θ, keeping the laser and sample fixed. The signal ratio is defined as $S_{\mathrm{REM}}/S_{\mathrm{ref}}$, where S_{REM} and S_{ref} are intensities detected from the REM and plain fluorescence sample. Experimentally, we found a maximum ratio of 17.6 for $\theta = \phi = 0°$, and FWHM angular divergence of the REM beam of approximately 2.6°. Note that the beam profile was convolved with the aperture of the imaging system (diameter, $a = 21\,\mathrm{mm}$).

The signal ratio dependency on ϕ is shown in Fig. 2(c). This ratio remains flat at the maximum value of 17.6, and drops steeply at a cutoff value of ~18°. The REM effect cutoff is explained by the sphere excitation light focusing above the fluorescent substrate at $\phi > 18°$, resulting in diminished fluorescence excited in the voxel.

The simulation captured the shape of the narrow REM cone well [Fig. 2(b)], with a maximum ratio of 24 when using the same collection angle as in the experiment. Since the simulation was confined to a single bead, this ratio was higher than that obtained in the experiment, which represented an averaging over an area with an estimated 70%–80% bead fill factor.

Consider the case of excitation/detection coalignment and normal incidence ($\theta = \phi = 0°$). The effective excitation intensity at the focal point of the sphere can be expressed as $I_{\mathrm{ex,focus}} = L_{\mathrm{in}}(R/r)^2 I_{\mathrm{ex}}$, where I_{ex} is the excitation intensity incident on the sample, L_{in} is the fraction of transmitted light accounting for sphere reflection and scattering losses, R is the bead radius, and r is the radius of the focal region, which is assumed circular. The emitted fluorescence from this region was subsequently collected and projected from the bead surface, with associated losses accounted for by L_{out} (the fraction of the emitted light found in the REM beam). We attributed a separate "observation function" $f(d, a)$ to both the REM and plain fluorescent samples that quantified the fluorescence measured by the CCD camera as a function of d and a. The ratio of the REM and plain fluorescence signals is estimated as

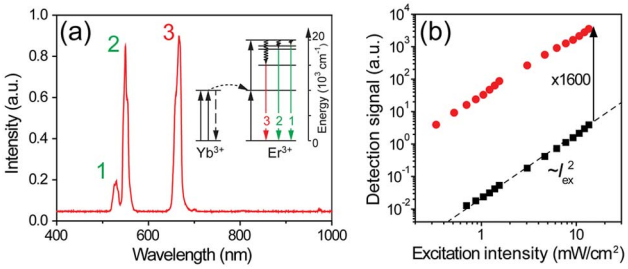

Fig. 3. (Color online) (a) Luminescence emission spectrum for the UCP. (b) REM signal (circles) and reference UCP signal (squares) as a function of the excitation intensity.

$$\frac{S_{\mathrm{REM}}}{S_{\mathrm{ref}}} = L_{\mathrm{in}} L_{\mathrm{out}} \frac{f_{\mathrm{REM}}}{f_{\mathrm{ref}}}, \tag{1}$$

where the material fluorescence properties (quantum yield, absorption cross section) cancel out. The ray tracing simulation allowed quantification of the parameters for the specific experimental setup; $L_{\mathrm{in}} \approx 0.81$, $L_{\mathrm{out}} \approx 0.43$, $f_{\mathrm{REM}} \approx 0.14$, and $f_{\mathrm{ref}} \approx 0.002$, which, using Eq. (1), gives 24.4, in close agreement with the overall simulation result.

By replacing the fluorescent substrate with a nonlinear optical material substrate, such as UPC [6], an enhancement of the REM effect is envisaged due to the local excitation intensity increase by a factor of $\sim(R/r)^2$ in the voxel, and the emission signal dependence on I_{ex}^2, so that emission is primarily excited in the voxel.

In order to demonstrate this effect experimentally, a high-refractive-bead REM device was placed on an ~1 mm thick UCP substrate comprised of polydisperse 5 μm particles of inorganic crystals doped with Yb^{3+} sensitizer ions and Er^{3+} activator ions (Luminophore, Fryazino, Russia). The emission spectrum excited by a 980 nm laser (LD980-01CW, CXCH-Photonics) is shown in Fig. 3(a). Nonradiative energy transfer from the sensitizer to the activator ions and subsequent collective energy transfer upconversion results in two-photon absorption, with re-emission in the green and red spectral bands [6].

Both the REM and plain UCP substrates were imaged using the CCD camera placed at a 2 m distance ($\theta = \phi = 0°$) from the sample. Using a calibrated adjustable laser power supply and neutral density filters, we measured the retroemitted luminescence as a function of the excitation intensity for both the REM and plain UCP substrates. The laser–sample distance was 50 cm, and a diffuser was used to obtain a spatially uniform excitation field.

Figure 3(b) presents a log–log plot of the average luminescence signal from both the REM and the plain UCP substrates versus I_{ex}, which exhibits quadratic dependence over the measured range. The ratio of REM to UCP signal was found to be as high as 1000–2000, depending on the bead quality. An example is plotted in Fig. 3(b) (red circles), where the intensity measured as an average over the bead surface was 1600-fold that of an average over the plain UCP substrate.

Since the signal emission depends on $S_{\mathrm{em,focus}} \sim I_{\mathrm{ex,focus}}^2$, we have the following expression for the emission signal at the focal point, with the optical losses included:

$$S_{\mathrm{em,focus}} \sim L_{\mathrm{in}}^2 \left(\frac{R}{r}\right)^4 I_{\mathrm{ex}}^2. \tag{2}$$

As before, the emitted light was subsequently collected and collimated by the sphere. In our simplified model, the ratio between REM and plain UCP signals at a distant observation point $d = 2$ m, becomes

$$\frac{S_{\mathrm{REM,UCP}}}{S_{\mathrm{ref,UCP}}} = L_{\mathrm{out}} L_{\mathrm{in}}^2 \left(\frac{R}{r}\right)^2 \frac{\kappa f_{\mathrm{REM}}}{f_{\mathrm{ref}}}, \tag{3}$$

where a correction factor κ accounts for the nonnegligible refractive index dispersion at the excitation and emission wavelengths, 980 and 550 nm, respectively. From the simulation we find $\kappa = 0.2$ (assuming a 5% reduction in refractive index for the IR [10]), such that $\kappa f_{\mathrm{REM}} = 0.028$. The estimated ratio $R/r \sim 30$ for the current setup was primarily determined by the light source extension (~5 mm), giving a contrast ratio [Eq. (3)] of ~3500, which is reasonably close to the experimentally observed value.

In conclusion, we have characterized a REM device comprising high-refractive-index beads mounted on a luminescent substrate. The REM effect allowed luminescence detection at large distances due to the autocollimation of the emitted light in the opposite direction of the collimated excitation beam. A REM device placed on a nonlinear optical material (UPC) substrate was demonstrated to exhibit over 3 orders of magnitude signal contrast enhancement. Useful practical applications of this technique are envisaged in fields of remote sensing and molecular labeling based on upconverting nanophosphors.

References

1. M. Rajadhyaksha, S. Gonzalez, J. M. Zavislan, R. R. Anderson, and R. H. Webb, J. Invest. Dermatol. **113**, 293 (1999).
2. R. Juskaitis, T. Wilson, M. A. A. Neil, and M. Kozubek, Nature **383**, 804 (1996).
3. W. R. Zipfel, R. M. Williams, and W. W. Webb, Nat. Biotechnol. **21**, 1369 (2003).
4. H. Tanaka and S. Tanaka, "Apparatus for detecting modulated informations from emitted light turned by an object," U.S. patent 5,091,636 (February 25, 1992).
5. Z. Wang, W. Guo, L. Li, B. Luk'yanchuk, A. Khan, Z. Liu, Z. Chen, and M. Hong, Nat. Commun. **2**, 218 (2011).
6. R. H. Page, K. I. Schaffers, P. A. Waide, J. B. Tassano, S. A. Payne, W. F. Krupke, and W. K. Bischel, J. Opt. Soc. Am. B **15**, 996 (1998).
7. H. X. Mai, Y. W. Zhang, R. Si, Z. G. Yan, L. D. Sun, L. P. You, and C. H. Yan, J. Am. Chem. Soc. **128**, 6426 (2006).
8. S. W. Wu, G. Han, D. J. Milliron, S. Aloni, V. Altoe, D. V. Talapin, B. E. Cohen, and P. J. Schuck, Proc. Natl. Acad. Sci. USA **106**, 10917 (2009).
9. J. C. Boyer and F. van Veggel, Nanoscale **2**, 1417 (2010).
10. A. Masuno, H. Inoue, J. Yu, and Y. Arai, J. Appl. Phys. **108**, 063520 (2010).

Optics Letters

BACK TO RESULTS

Basic Description | Other Editions/ Formats | Abstracting/ Indexing & Article Access | Publisher & Ordering Information | Advertising, Rights, Demographics | Reviews

JCR Web

Click highlighted text for a new search on that item.

Table of Contents:	Click here to view
ISSN:	0146-9592
Title:	Optics Letters Additional Title Information
Publishing Body:	Optical Society of America
Country:	United States
Status:	Active
Start Year:	1977
Frequency:	Semi-monthly
Volume Ends:	Jan - Dec
Document Type:	Journal; Academic/Scholarly
Refereed:	Yes
Abstracted / Indexed:	Yes
Media:	Print
Alternate Edition ISSN:	1539-4794
Size:	Standard
Language:	Text in English
Price:	USD 2,650 combined subscription per year domestic to institutions (Print & Online Eds.) USD 2,735 combined subscription per year in Canada to institutions (Print & Online Eds.) USD 2,840 combined subscription per year elsewhere to institutions (Print & Online Eds.) (effective 2010)
Subject:	PHYSICS - OPTICS
Dewey #:	535
LC#:	QC350
CODEN:	OPLEDP
Special Features:	Illustrations
Article Index:	Index Available
Composition:	Web, offset
Editor(s):	Alan E Willner (Editor-in-Chief)
URL:	http://www.opticsinfobase.org/ol/journal/ol/about.cfm
Description:	Covers the latest research in optical science, including atmospheric optics, quantum electronics, fourier optics, integrated optics, and fiber optics.

ADDITIONAL TITLE INFORMATION

Alternate Title:	Medline Abbreviated title: Opt Lett; Abbreviated title: O L

Back to Top

Add this item to: (select a list) + ADD

Request this title: I'd like to request this title. GO

Corrections: Submit corrections to Ulrich's about this title. GO

Publisher of this title? If yes, click GO! to contact Ulrich's about updating your title listings in the Ulrich's database. GO

Print • Download • E-mail

Back to Top